Hidden security threat identification: A reduced order model for the rapid computation of object characterisations

B. A. Wilson*, P. D. Ledger

Zienkiewicz Centre for Computational Engineering, College of Engineering,
Swansea Bay Campus, Swansea, SA1 8EN UK.
b.a.wilson@swansea.ac.uk, p.d.ledger@swansea.ac.uk

Abstract

This work presents computational results of a reduced order model for the rapid calculation of conducting object characterisations as a function of frequency in metal detection. Such characterisations are called their spectral signature. We present a brief description of the eddy-current model and the magnetic polarizability tensor (MPT) used for our object characterisations. The transmission problem required for the computation of the MPT and its discretisation is then described followed by a summary of the reduced order model. As an illustration of the capabilities of the approach for characterising realistic objects, we show MPT spectral signatures of a British £1 coin.

Key words: *Metal detection; Magnetic polarizability tensor; Reduced order model; Object classification.*

1 Introduction

The location and identification of hidden conducting security threats in metal detection is an important yet difficult task. Recently, there has been considerable interest in using the magnetic polarizabilty tensor (MPT), to characterise conducting permeable targets [1, 2, 3, 4]. Considering the frequency (or spectral) behaviour of the MPT, henceforth called its spectral signature, offers significant advantages to simple thresholding techniques, namely, information about a hidden object's size, shape, conductivity and permeability. This is because the associated metal detection inverse problem becomes one of classifying an object according to its MPT spectral signature. We are interested in machine learning approaches for the classification and to do this training data is required. The purpose of this paper is to present computational results of a recently implemented reduced order model [5] for practical examples to illustrate how the training data can be generated. The paper is organised as follows: in Section 2, the eddy current model and asymptotic expansion, which leads to the explicit expression of the MPT, are briefly reviewed. In Section 3, the full order model along with the finite element discretisation are defined. This is followed, in Section 4, with the reduced order model (ROM) scheme used. Section 5 presents numerical results for a British £1 coin.

2 The eddy-current model and asymptotic expansion

The eddy-current model is a low frequency approximation of the Maxwell system in which the displacement currents are neglected. For the case of a small conducting object $B_\alpha := \alpha B + \boldsymbol{z}$, where α is the object size, B is its shape and $\boldsymbol{z}$ is its position, in a non conducting medium B_α^c the model is described by

$$\nabla \times \boldsymbol{E}_\alpha = \mathrm{i}\omega\mu \boldsymbol{H}_\alpha, \qquad \nabla \times \boldsymbol{H}_\alpha = \boldsymbol{J}_0 + \sigma \boldsymbol{E}_\alpha, \tag{1}$$

where $\boldsymbol{E}_\alpha$ and $\boldsymbol{H}_\alpha$ are the electric and magnetic interaction fields, respectively, $\boldsymbol{J}_0$ is an external current source, $\mathrm{i} := \sqrt{-1}$, ω is the angular frequency and μ, σ are the magnetic permeability and electric conductivity respectfully and are defined as

$$\mu(\boldsymbol{x}) = \begin{cases} \mu_* & \boldsymbol{x} \in B_\alpha \\ \mu_0 & \boldsymbol{x} \in B_\alpha^c \end{cases}, \qquad \sigma(\boldsymbol{x}) = \begin{cases} \sigma_* & \boldsymbol{x} \in B_\alpha \\ 0 & \boldsymbol{x} \in B_\alpha^c \end{cases}, \tag{2}$$

where $\mu_0 = 4\pi \times 10^{-7}$H/m and is the permeability of free space. Practical metal detectors measure $(\boldsymbol{H}_\alpha - \boldsymbol{H}_0)(\boldsymbol{x})$ and a traditional approach to solving the inverse problem of identifying the object

would involve determining $\mu(\boldsymbol{x})$ and $\sigma(\boldsymbol{x})$ and using these to infer the position and object shape, which is expensive. Instead we follow an alternative approach in which objects are characteriesed by MPTs. We accomplish this by using the asymptotic formula derived by Ammari et al [1], which has been simplified by Ledger and Lionheart [2] to

$$(\boldsymbol{H}_\alpha - \boldsymbol{H}_0)(\boldsymbol{x})_i = (\boldsymbol{D}^2_{\boldsymbol{x}} G(\boldsymbol{x}, \boldsymbol{z}))_{ij} (\mathcal{M}[\alpha B, \omega])_{jk} (\boldsymbol{H}_0(\boldsymbol{z}))_k + O(\alpha^4), \tag{3}$$

as $\alpha \to 0$ where $\mathcal{M}[\alpha B, \omega] = (\mathcal{M}[\alpha B, \omega])_{ij} \boldsymbol{e}_i \otimes \boldsymbol{e}_j$ is the (complex symmetric) rank 2 MPT, $\mathbf{e}$ is unit basis vector and $\boldsymbol{D}^2_{\boldsymbol{x}} G(\boldsymbol{x}, \boldsymbol{z})$ is the Hessian of the free space Laplace Green's function $G(\boldsymbol{x}, \boldsymbol{z}) = 1/(4\pi|\boldsymbol{x} - \boldsymbol{z}|)$.

3 Full order model and finite element discretisation

Our intrest lies in the computation of $(\mathcal{M}[\alpha B, \omega])_{ij}$ as a function of ω that can be obtained from the solution of the transmission problem

$$\nabla \times \mu_*^{-1} \nabla \times \boldsymbol{\theta}_i^{(1)} - \mathrm{i}\nu(\tilde{\boldsymbol{\theta}}_i^{(0)} + \boldsymbol{\theta}_i^{(1)}) = \mathbf{0} \qquad \text{in } B, \tag{4a}$$

$$\nabla \times \mu_0^{-1} \nabla \times \boldsymbol{\theta}_i^{(1)} = \mathbf{0} \qquad \text{in } B^c, \tag{4b}$$

$$\nabla \cdot \boldsymbol{\theta}_i^{(1)} = 0 \qquad \text{in } B^c, \tag{4c}$$

$$[\boldsymbol{n} \times \boldsymbol{\theta}_i^{(1)}]_\Gamma = \mathbf{0} \qquad \text{on } \Gamma, \tag{4d}$$

$$[\boldsymbol{n} \times \mu^{-1} \nabla \times \boldsymbol{\theta}_i^{(1)}]_\Gamma = \mathbf{0} \qquad \text{on } \Gamma, \tag{4e}$$

$$\boldsymbol{\theta}_i^{(1)} = \boldsymbol{O}(|\boldsymbol{\xi}|^{-1}) \qquad \text{as } |\boldsymbol{\xi}| \to \infty, \tag{4f}$$

where $[\cdot]_\Gamma$ denotes the jump, $\Gamma := \partial B$, $\nu := \alpha^2 \omega \mu_0 \sigma_*$ and $\tilde{\boldsymbol{\theta}}_i^{(0)} := \boldsymbol{\theta}_i^{(0)} + \boldsymbol{e}_i \times \boldsymbol{\xi}$ is a source term independent of ω. We apply `NGSolve` to obtain discrete finite element approximations to (4) using Nédélec *hp* version finite elements, leading to the linear system of equations of dimension N_d [5]

$$\mathbf{A}(\omega)\mathbf{q}(\omega) = \mathbf{r}(\boldsymbol{\theta}^{(0,hp)}, \omega), \tag{5}$$

which must be solved for each ω where $\boldsymbol{\theta}^{(0,hp)}$ denotes the finite element (FE) solution of $\boldsymbol{\theta}^{(0)}$. Note we have also dropped the index i for simplicity.

4 Reduced order model

To reduce the computational cost of repeatedly solving (5) for each value of ω, we use projection based proper orthogonal decomposition (PODP) to create a much smaller surrogate problem as described in [5] and references therein. We briefly summarise the steps below: Equation 5 is solved for $\mathbf{q}(\omega_i), i = 1, \ldots, N$ and the solution vectors stored as

$$\mathbf{D} := [\mathbf{q}(\omega_1), \mathbf{q}(\omega_2), ..., \mathbf{q}(\omega_N)] \ \in \ \mathbb{C}^{N_d \times N}. \tag{6}$$

We then apply a truncated singular value decomposition to obtain

$$\mathbf{D} \approx \mathbf{D}^M = \mathbf{U}^M \mathbf{\Sigma}^M (\mathbf{V}^M)^*, \tag{7}$$

where $\mathbf{U}^M \in \mathbb{C}^{N_d \times M}$, $\mathbf{\Sigma}^M \in \mathbb{R}^{M \times M}$, $(\mathbf{V}^M)^* \in \mathbb{C}^{M \times N}$, $*$ denotes the Hermission and where $M \leq N$ is determined by the tolerance of truncation. We use $\mathbf{U}^M$ to project problem (5) to a lower dimensional space, resulting in a reduced system of dimension $M \ll N_d$,

$$\mathbf{A}^M(\omega)\mathbf{p}(\omega) = \mathbf{r}^M(\omega), \tag{8}$$

where $\mathbf{A}^M(\omega) := (\mathbf{U}^M)^* \mathbf{A}(\omega) \mathbf{U}^M$ and $\mathbf{r}^M(\omega) := (\mathbf{U}^M)^* \mathbf{r}(\omega)$. Then, we obtain an approximate solution $\mathbf{q}(\omega) \approx \mathbf{U}^{\mathrm{M}} \mathbf{p}(\omega)$, from which, by combining with the FE basis functions, we can compute $(\mathcal{M}[B, \omega])^{PODP}_{ij}$. We have also obtained output certificate bounds $|\mathrm{Re}((\mathcal{M}[B, \omega])_{ij}$ $- (\mathcal{M}[B, \omega])^{PODP}_{ij})| \leq (\Delta[\omega])_{ij}$ and $|\mathrm{Im}((\mathcal{M}[B, \omega])_{ij} - (\mathcal{M}[B, \omega])^{PODP}_{ij})| \leq (\Delta[\omega])_{ij}$ for the accuracy $(\mathcal{M}[B, \omega])^{PODP}_{ij}$ with respect $(\mathcal{M}[B, \omega])_{ij}$ obtained by the full order FE model [5].

5 Numerical results

To illustrate the practical capabilities of the approach, we apply it to the characterisation where $B_\alpha = \alpha B$ is a British £1 coin, The coin has a diameter of 23.43mm (point to point) and a thickness of 2.88mm, the inner portion of the coin is made from nickel plated brass and the outer being a nickel brass alloy [6], which we have modelled to have conductivities of $\sigma_* = 1.63 \times 10^7$ S/m and $\sigma_* = 5.26 \times 10^6$ S/m, respectively, with both parts of the coin having a relative permeability $\mu_*/\mu_0 = 1$. We have discretised this using a 30645 unstructured tetrahedral element mesh with $p = 4$ elements, for which the solution was found to be converged under p-refinement across the range of frequencies of interest.

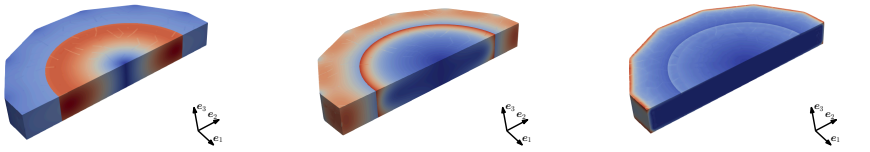

(a) $|\boldsymbol{J}^e|$ for $\omega = 10^3$ rad/s. (b) $|\boldsymbol{J}^e|$ for $\omega = 10^5$ rad/s. (c) $|\boldsymbol{J}^e|$ for $\omega = 10^7$ rad/s.

Figure 1: A £1 coin modelled with $\mu_*/\mu_0 = 1$ and conductivities $\sigma_* = 1.63 \times 10^7$ S/m and $\sigma_* = 5.26 \times 10^6$ S/m for the inner and outer part of the coin, respectively: eddy-currents $\boldsymbol{J}^e = \mathrm{i}\omega\sigma_*\boldsymbol{\theta}_3^{(1)}$ for the inner and outer portions of the coin respectively for different values of ω, (a) $\omega = 10^3$ rad/s, (b) $\omega = 10^5$ rad/s, (c) $\omega = 10^7$ rad/s.

In Figure 1, we observe, as ω, increases that the eddy currents become confined to a thin layer close to the outer edge and the material interface. This is associated with the small skin depth at high frequencies and requires an accurate discretisation. For the inner interface this occurs at a lower frequency, due to its higher conductivity [5]. The spectral signature of the MPT is considered next. We use the full order FE model described above to generate solution snapshots at $N = 13$ logarithmically spaced frequencies such that $10^1 \leq \omega \leq 10^{10}$ rad/s. The PODP approach using $M = N$ is then applied to compute the MPT spectral signature at 161 points leading to the result for $\mathcal{M}[\alpha B, \omega]$ shown in Figure 2.

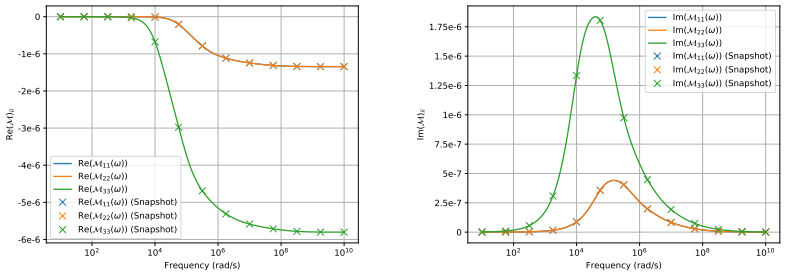

(a) $\mathrm{Re}(\mathcal{M}[\alpha B, \omega])_{ii}$. (b) $\mathrm{Im}(\mathcal{M}[\alpha B, \omega])_{ii}$.

Figure 2: A £1 coin modelled with $\mu_*/\mu_0 = 1$ and conductivities $\sigma_* = 1.63 \times 10^7$ S/m and $\sigma_* = 5.26 \times 10^6$ S/m for the inner and outer part of the coin, respectively: diagonal coefficients for (a) the real part and (b) the imaginary part of $\mathcal{M}[\alpha B, \omega]$.

Due to the coin's reflectional and rotational symmetries, its non-zero independent coefficients are $(\mathcal{M}[\alpha B, \omega])_{11} = (\mathcal{M}[\alpha B, \omega])_{22}$ and $(\mathcal{M}[\alpha B, \omega])_{33}$ and the MPT is diagonal. In Figure 3, we show the certificates bounds $(\Delta[\omega])_{ii}$ that are computed at run time of the PODP for $M = N = 25$.

These give creditability in the ROM, without the need to repeat full order solutions. Note that tighter bounds can be obtained by increasing N.

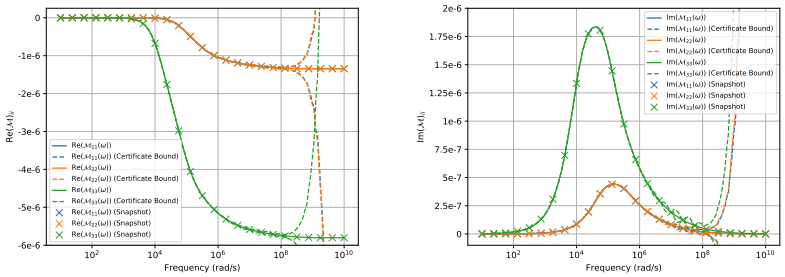

(a) $\mathrm{Re}(\mathcal{M}[\alpha B, \omega])_{ii}$. (b) $\mathrm{Im}(\mathcal{M}[\alpha B, \omega])_{ii}$.

Figure 3: A £1 coin modelled with $\mu_*/\mu_0 = 1$ and conductivities $\sigma_* = 1.63 \times 10^7$ S/m and $\sigma_* = 5.26 \times 10^6$ S/m for the inner and outer part of the coin, respectively: certificate bounds $(\Delta[\omega])_{ii}$ for (a) the real part and (b) the imaginary part of $(\mathcal{M}[\alpha B, \omega])_{ii}$.

The PODP with $N = 13$ took 18:01 minutes where as the full order FE model took 2:04:43 hours for the same MPT spectral signature, offering a saving of 86%. The solver time is clock time and all the computations were made in a cluster node using a machine Bull Sequana X440-E5 2 x Octa-Core (3.2 GHz) Xeon Gold v5 6134 and using a parallel pool of 16 workers.

The talk will also present results of object characterisations for both threat (e.g. guns and knives) as well as non-threat objects (e.g. coins).

Acknowledgments

The authors gratefully acknowledge the continued financial support received from EPSRC in the form of a DTP studentship with project reference number 2129099 and grant EP/R002134/1.

References

[1] H. Ammari, J. Chen, Z. Chen, D. Volkov, and H. Wang (2014): *Target detection and characterization from electromagnetic induction data.* J. Math. Pures Appl. 101(1), 54-75.

[2] P. D. Ledger and W. R. B. Lionheart (2014): *Characterising the shape and material properties of hidden targets from magnetic induction data.* IMA Journal of Applied Mathematics 80(6), 1776-1798.

[3] P. D. Ledger and W. R. B. Lionheart (2018): *An explicit formula for the magnetic polarizability tensor for object characterization.* IEEE Transactions on Geoscience and Remote Sensing 56(6), 3520-3533.

[4] P. D. Ledger and W. R. B. Lionheart (2020): *The spectral properties of the magnetic polarizability tensor for metallic object characterisation.* Mathematical Methods in the Applied Sciences, 43, 78-113.

[5] B. A. Wilson and P. D. Ledger (2020): *Efficient computation of the magnetic polarizability tensor spectral signature using POD.* `https://arxiv.org/abs/2001.07629`.

[6] Royal Mint: One Pound Coin. `https://www.royalmint.com/discover/uk-coins/coin-design-and-specifications/one-pound-coin/` (accessed on 8/03/2020)